Science Advances
AAAS

Supplementary Materials for

Crowder-directed interactions and conformational dynamics in multistimuli-responsive intrinsically disordered protein

Rajkamal Balu *et al.*

Corresponding author: Namita Roy Choudhury, namita.choudhury@rmit.edu.au; Naba K. Dutta, naba.dutta@rmit.edu.au

Sci. Adv. **8**, eabq2202 (2022)
DOI: 10.1126/sciadv.abq2202

This PDF file includes:

S1: Compilation of the reported results for intrinsically disordered proteins (IDPs) under macromolecular crowding conditions.

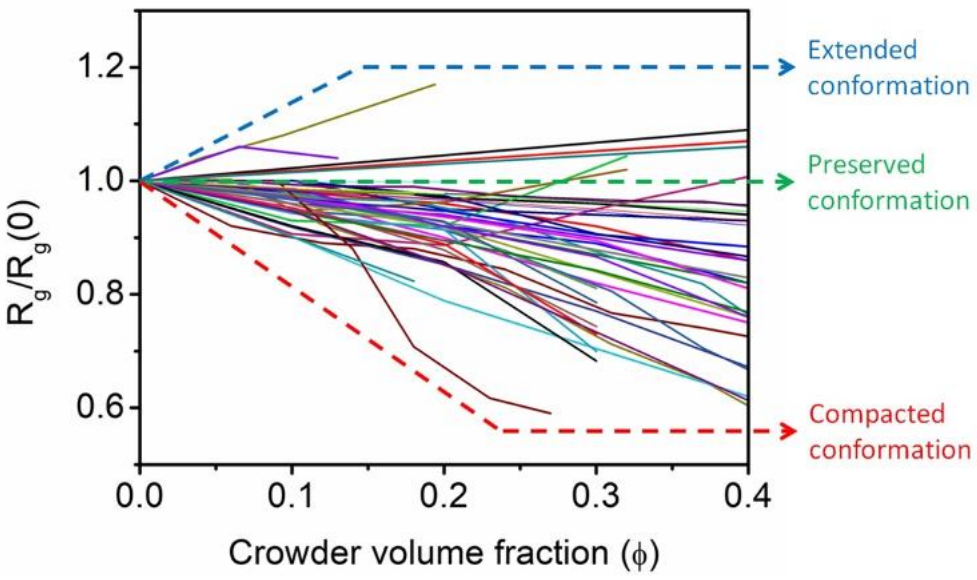

Figure S1. Compilation of the reported results for intrinsically disordered proteins (IDPs) under macromolecular crowding conditions. The radius of gyration (R_g) of IDPs in the absence of crowders, $R_g(0)$, is used to normalize the data for IDPs of varying sizes in order to show the percentage change in R_g with crowder volume fraction. The dotted lines are an indicative envelope of the reported trends.

S2: Structural consensus and amino acid repeat sequence in rec1-resilin.

MHHHHHHPEPPVNSYLPPSDSYGAPGQSGPGGRPSDSYGAPGGGNGGRPS	50
DSYGAPGQGQGQGQGQGGYAGKPSDSYGAPGGGNGNGGRPSSSYGAPGGG	100
NGGRPSDTYGAPGGGNGGRPSDTYGAPGGGGNGNGGRPSSSYGAPGQGQG	150
NGNGGRPSSSYGAPGSGNGGRPSDTYGAPGGGNGGRPSDTYGAPGGGNNG	200
GRPSSSYGAPGGGNGGRPSDTYGAPGGGNGNGSGGRPSSSYGAPGQGQGG	250
FGGRPSDSYGAPGQNQKPSDSYGAPGSGNGNGGRPSSSYGAPGSGPGGRP	300
SDSYGPPASG	310

Figure S2. Amino acid sequence (single letter code) of Rec1-resilin. Rec1-resilin is a water soluble protein consists of 310 amino acid residues containing evolutionarily conserved oligopeptide repeats consisting of 18 copies of a 15-residue repeat consensus sequence: **GGRPSDSYGAPGGGN.**

S3: Structural details of the crowders used and rationale for the selection of the crowders

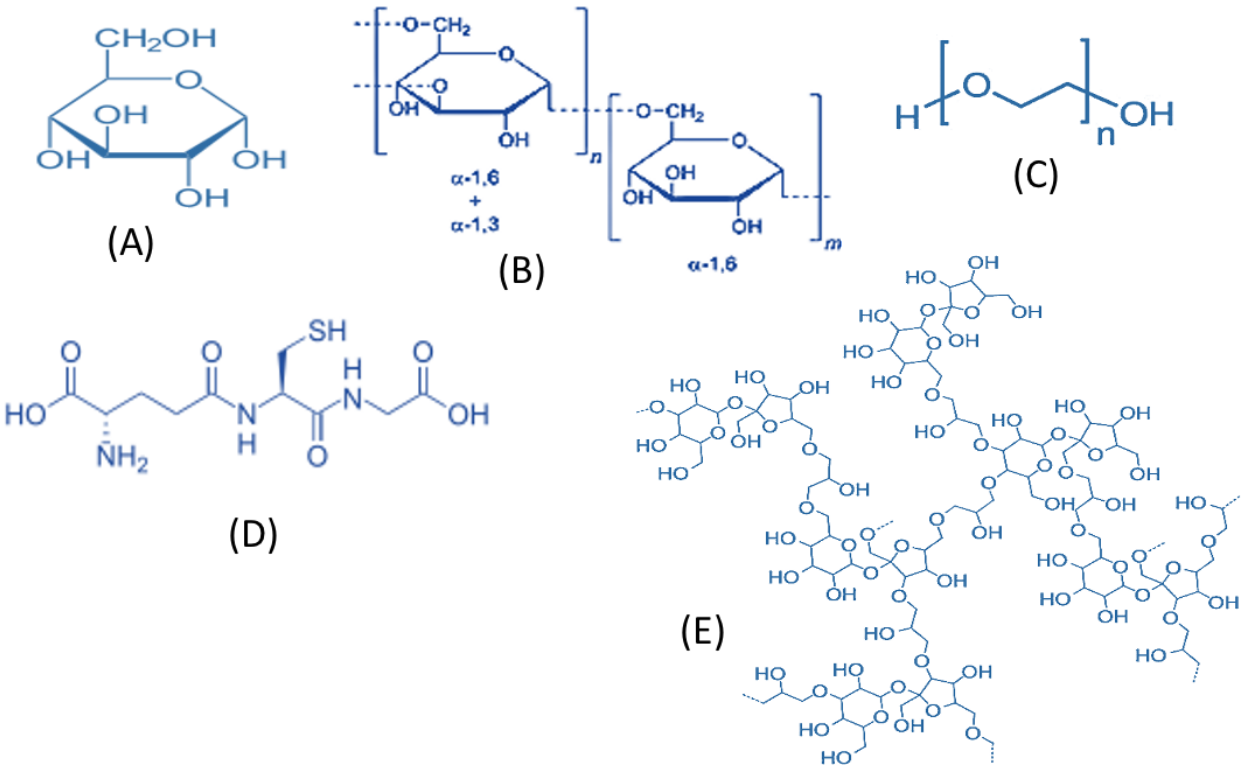

Figure S3. Structural details of the crowders used and rationale for the selection of the crowders. (A) Glucose, the most common monosaccharide. Glucose is essential for all organ systems because it fuels a variety of mechanisms that perform vital tasks. It is crucial for the tissues, erythrocytes, skeletal muscles, and brain. (B) Dextran, a complex branched glucan (polysaccharide derived from the condensation of glucose). Dextran is an important biomaterial with a very diverse application ranging from vaccines to prodrug nanoparticle /nanogel/ microsphere/micelle carrier for targeting drug delivery systems to infusion fluid. (C) Polyethylene glycol (PEG)- Applications of PEG include surface modification for controlled therapy release in medical devices, regenerative medicine, and cell culture. Small molecule drugs are PEGylated to maintain high drug loads, increase drug release function, slow blood drug clearance, increase full drug penetration into tumors, and enhance the medication's pharmacokinetic profile. In vitro tests frequently use PEG as a crowding agent to simulate densely packed cellular environments. PEG-coated viral vectors are utilised in gene therapy to avoid immune system inactivation. (D) Glutathione (GSH) is a tripeptide (γ-glutamyl-cysteinyl-glycine) glutamate residue. The most prevalent intracellular thiol (1–10 mmol/L), GSH, detoxifying reactive oxygen species and other

xenobiotics as well as transports amines and peptides through the plasma membrane (E) Ficoll® is a neutral, highly branched, high-mass hydrophilic polysaccharide. It is synthesized by crosslinking sucrose and epichlorohydrin, which results in a branching structure. The most popular application of Ficoll® is as a density gradient medium for the separation and isolation of eukaryotic cells as well as for the isolation of bacterial cells and organelles.

S4: Hydrodynamic diameter (D_h) and Zeta (ζ)-potential of D-Rec1 and crowding agents

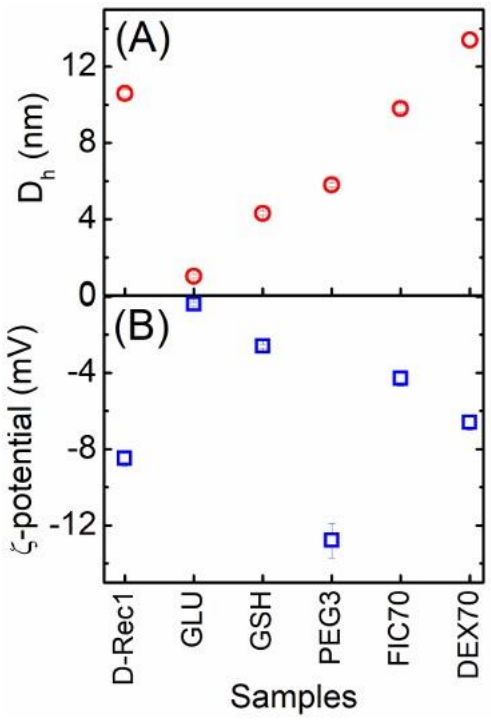

Figure S4. Hydrodynamic diameter and Zeta potential of D-Rec1 and crowding agents. (A) Hydrodynamic diameter (D_h) and (B) Zeta (ζ)-potential of 0.1 wt% D-Rec1 and crowding agents in 10 mM phosphate buffered saline (PBS) obtained using DLS. The data are presented as an average value with standard deviation from three measurement cycles.

S5: SAXS intensity profile (with model function fits) of crowding agents solutions

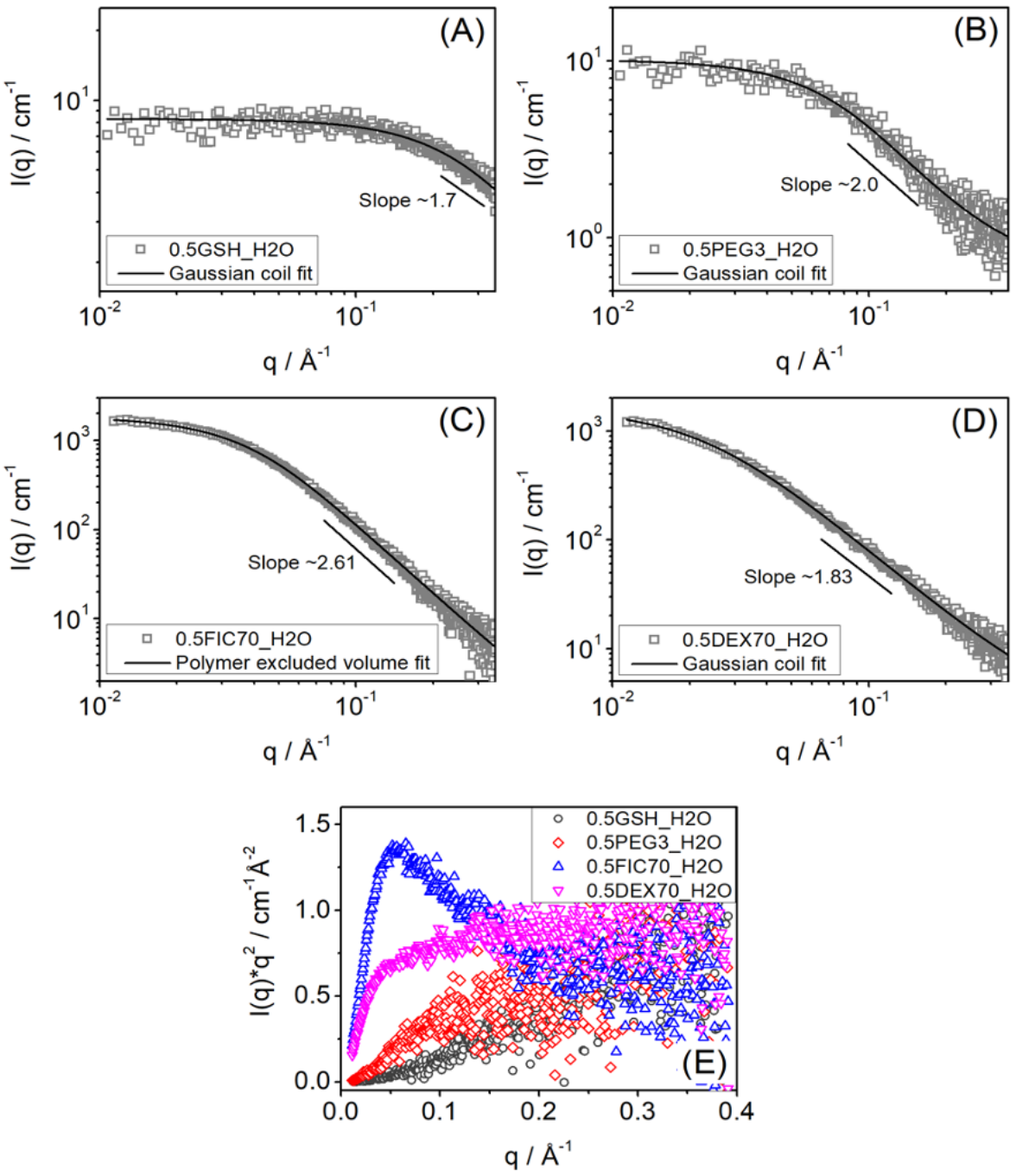

Figure S5. SAXS intensity profile with model function fits of 0.5 wt% crowding agents. (A) glutathione (GSH), (B) polyethylene glycol (PEG3), (C) Ficoll (FIC70) and (D) dextran (DEX70) in water. (E) Corresponding Kratky plot.

S6: Extended SANS intensity profile (with and without solvent contrast matching) of crowding agents

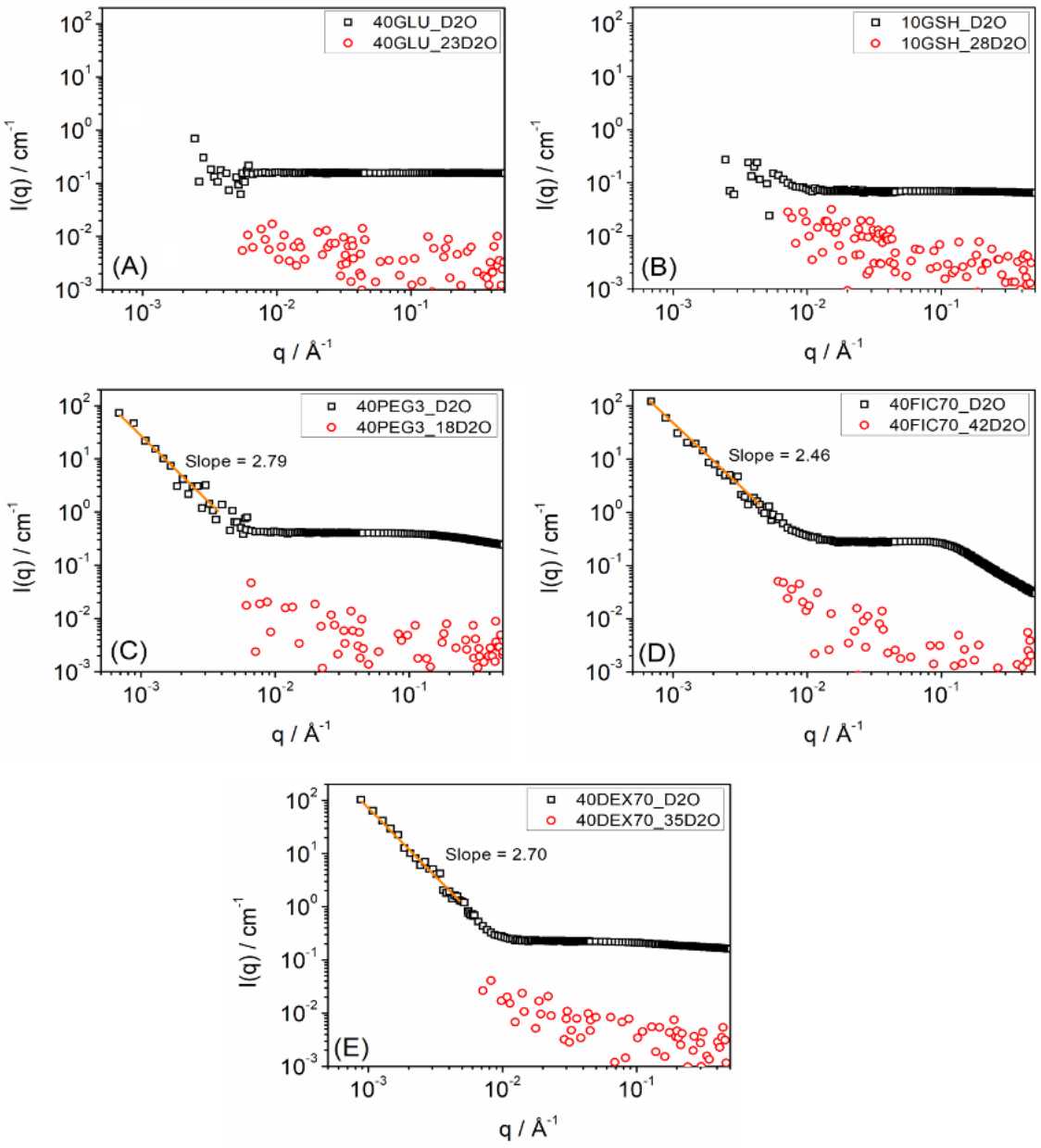

Figure S6. Extended SANS intensity profile with and without solvent contrast matching of crowding agents. (A) glucose (GLU), (B) glutathione (GSH), (C) polyethylene glycol (PEG3), (D) Ficoll (FIC70) and (E) dextran (DEX70) in 10 mM PBS at their maximum tested concentration.

S7: Kratky plot of 3.0 wt% D-Rec1 SANS data as a function of different crowding agent

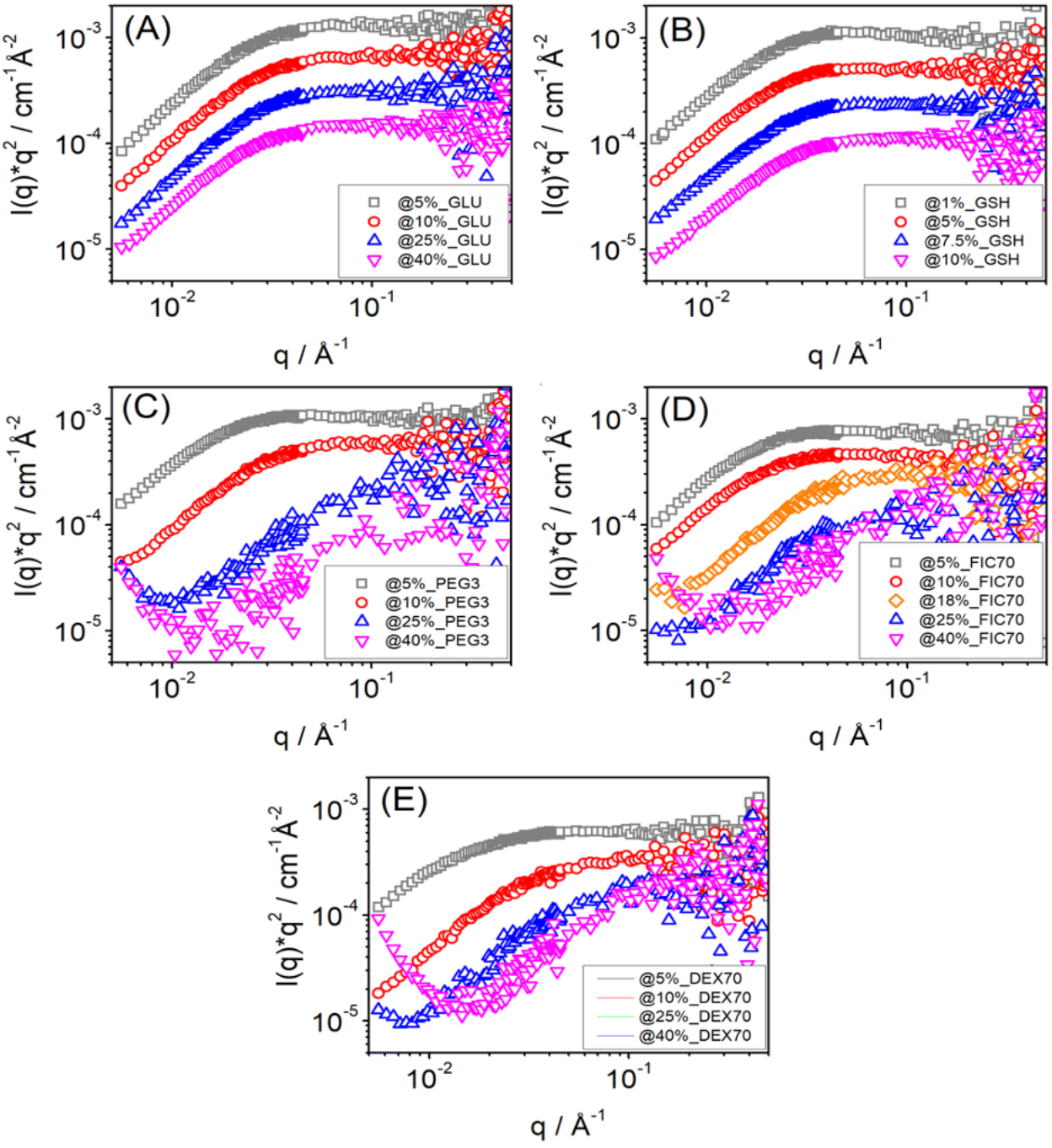

Figure S7. Kratky plot of 3.0 wt% D-Rec1 SANS data as a function of different crowding agent, with contrast matched to solvent, at different concentration. (A) glucose (GLU), (B) glutathione (GSH), (C) polyethylene glycol (PEG3), (D) Ficoll (FIC70), and (E) dextran (DEX70).

S8: Polymer excluded volume model fit to SANS data of 3.0 wt% D-Rec1 as a function of different crowding agent

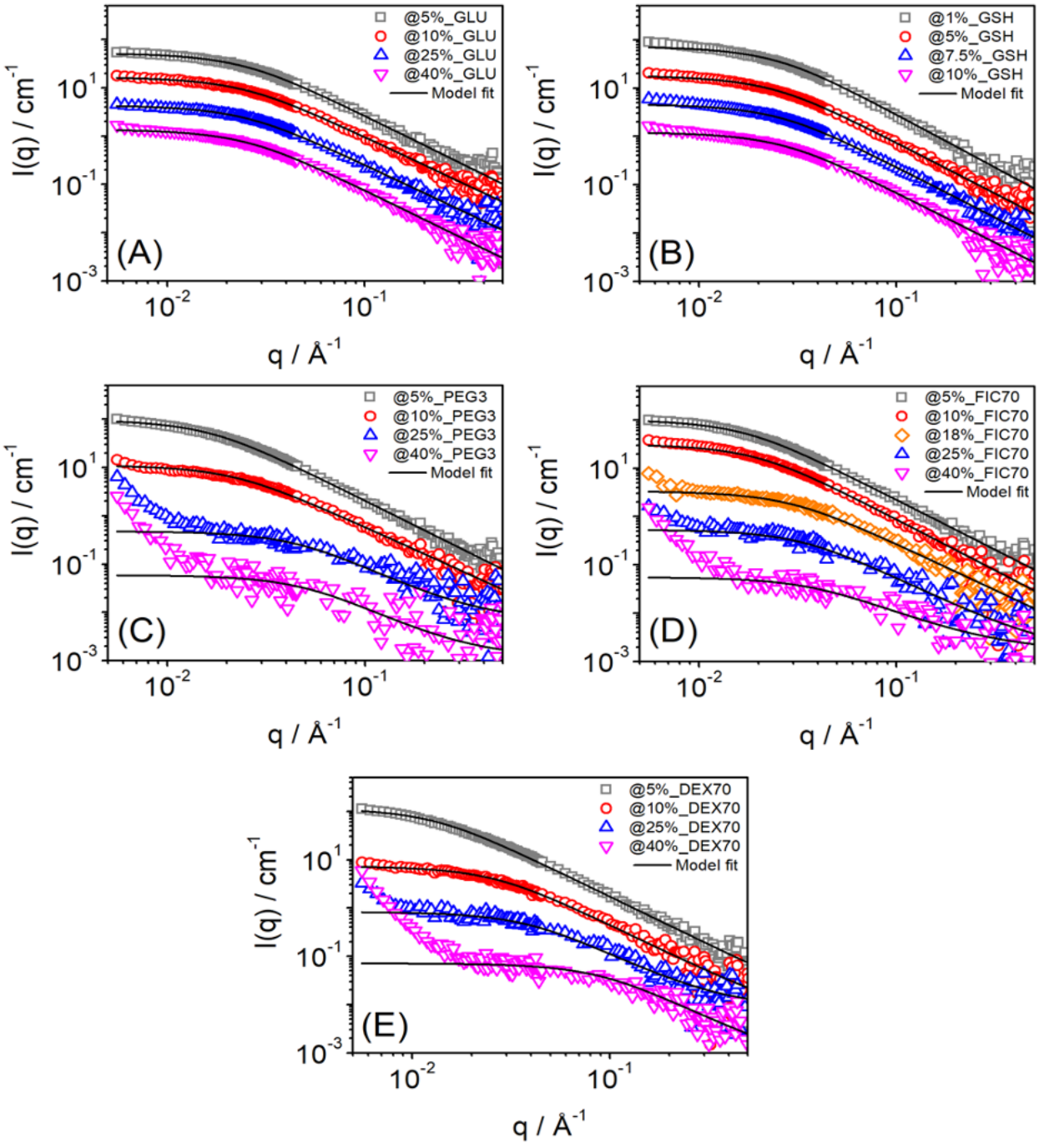

Figure S8. Polymer excluded volume model fit to SANS data of 3.0 wt% D-Rec1 as a function of different crowding agent, contrast matched to solvent, at different concentration. (A) glucose (GLU), (B) glutathione (GSH), (C) polyethylene glycol (PEG3), (D) Ficoll (FIC70), and (E) dextran (DEX70).

S9: Pair-distance distribution, P(r), curves of macromolecular crowding agents

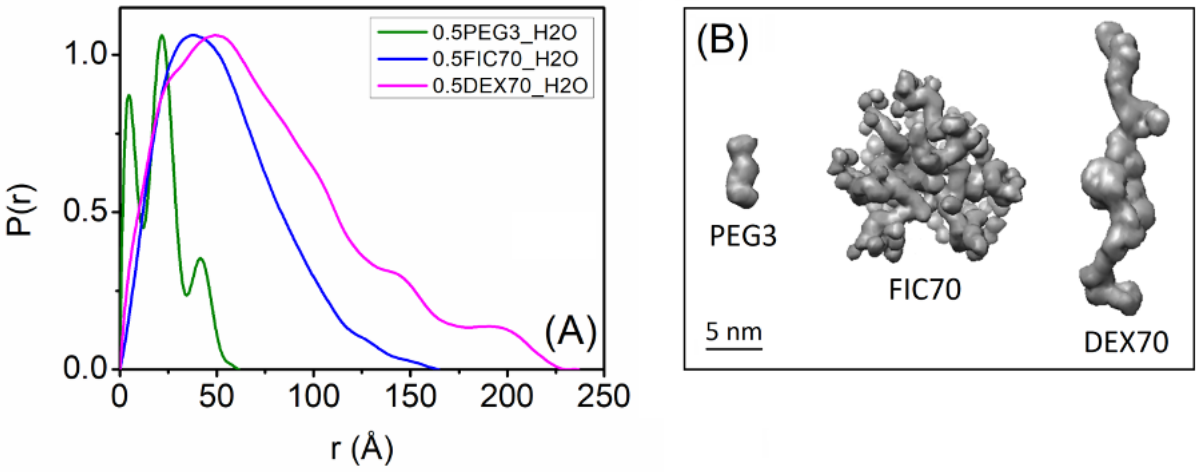

Figure S9. Pair-distance distribution, P(r), curves of macromolecular crowding agents. (A) polyethylene glycol (PEG3), Ficoll (FIC70) and dextran (DEX70) in water. (B) Corresponding *ab initio* shape reconstruction (one among an infinite possible ensemble) obtained using the GASBOR program and visualized (as an envelope structure) using the Chimera program.

S10: Photophysical properties of pure Rec1 and 8-Anilino-1-naphthalenesulfonic acid/Rec1-resilin (ANS/Rec1-resilin) complex at different molar ratios

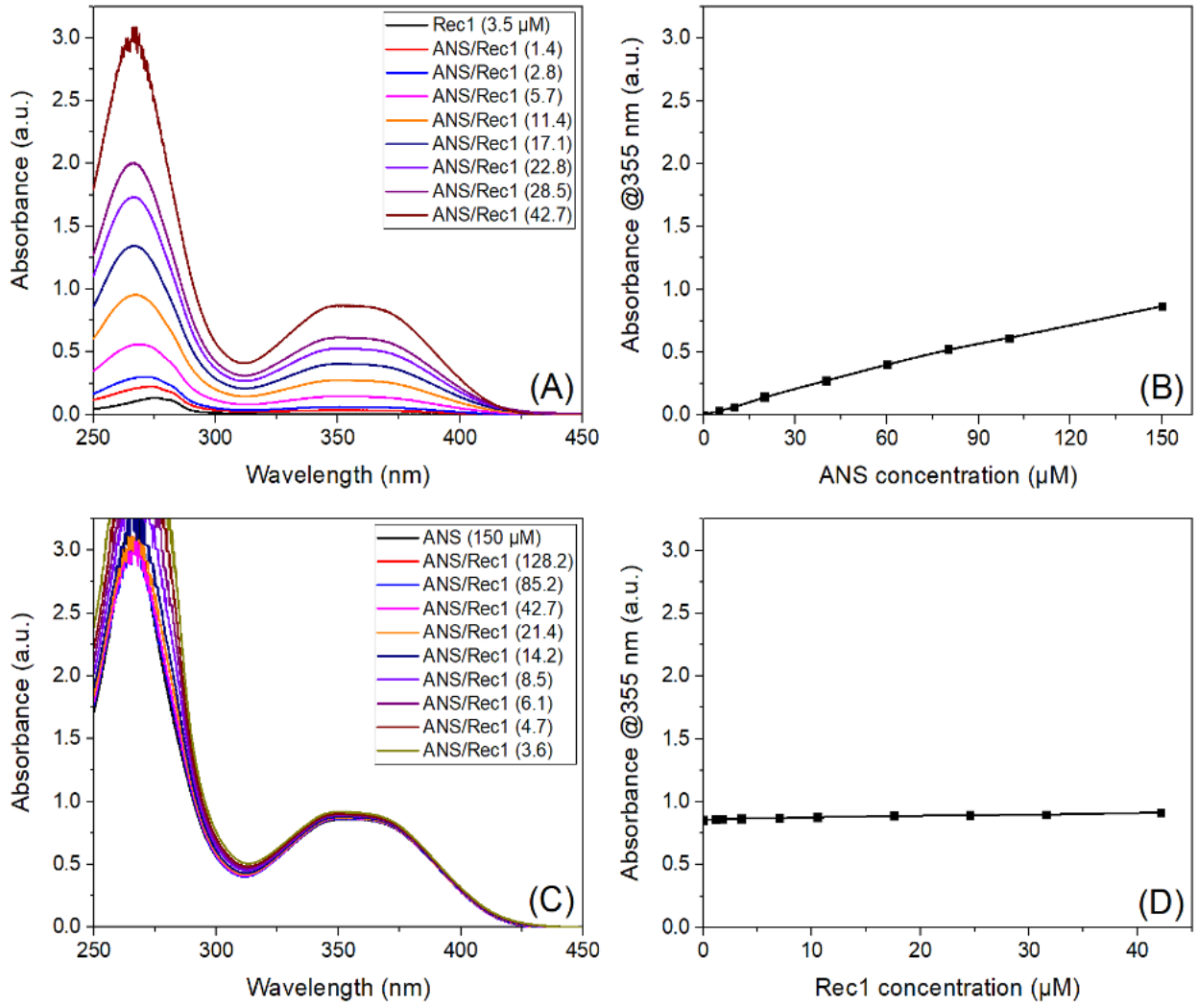

Figure S10. **Photophysical properties of pure Rec1 and 8-Anilino-1-naphthalenesulfonic acid/Rec1-resilin (ANS/Rec1-resilin) complex at different molar ratios.** (A) UV-Vis absorption spectra of pure Rec1-resilin and 8-Anilino-1-naphthalenesulfonic acid/Rec1-resilin (ANS/Rec1-resilin) complex at different molar ratios (with increase in ANS concentration). (B) UV-Vis absorption peak intensity (at 355 nm) plot as a function of ANS concentration at a fixed Rec1-resilin content. The peak intensity is linearly proportional to ANS concentration. (C) UV-Vis absorption spectra of pure ANS and ANS/Rec1 complex with increase in Rec1-resilin concentration at different molar ratios. (D) Corresponding UV-Vis absorption peak intensity plot. It is revealed that Rec1-resilin does not influence the peak position and intensity. ANS has been used to monitor protein conformational changes by binding to the hydrophobic regions of a protein. The absorption maximum of ANS observed at ~355nm was used as the excitation wavelength for the experiments.

S11: Assessment of surface hydrophobicity and Binding of ANS to Rec1-resilin

The two aromatic rings of ANS promote hydrophobic interactions and attach to hydrophobic cavities and areas on Rec1-resilin. This binding boosts the quantum yield and enhances λ_{max}. The data were analysed using Scatchard's equation and Hill's plot. Scatchard equation:

$$\frac{B}{L_F} = -\frac{B}{K_d} + \frac{R_T}{K_d} \qquad \text{(S1)},$$

where 'B' is the bound ligand and 'L_F' is free ligand; were used for analysis of the binding data. The plot of B/L_F vs B provides a straight line with R_T/K_d as the Y-intercept, R_T as the X-intercept, and $-1/K_d$ as the slope. K_d is the dissociation constant and R_T is the total receptor concentration. The smaller the dissociation constant, the more tightly bound the ligand is, or the higher the affinity between ligand and protein. The Hill slope analysis allows for the differentiation of cooperativity and multiple binding sites. The Hill equation accounts for the possibility that not all receptor sites are independent. According to Hill's Plot:

$$log\ [\frac{B}{R_T - B}] = n[logL_F] - log(K_d) \qquad \text{(S2)},$$

where, L_F is the free ligand concentration, 'R_T' is the total receptor concentration, and (R_{T-B}) is the free receptor concentration, and 'B' is the bound ligand and 'n' is the slope of the Hill plot and is also the average number of interacting sites. This equation is plotted as log $B/(R_{T-B})$ vs. log L_F where the Y-intercept is -log K_d and the slope n = the Hill coefficient. If the slope >1, the substrate-ligand interaction is positively cooperative, if the slope = 1, there is a single class of binding sites; and a slope <1 reflects negative cooperativity of the interaction.

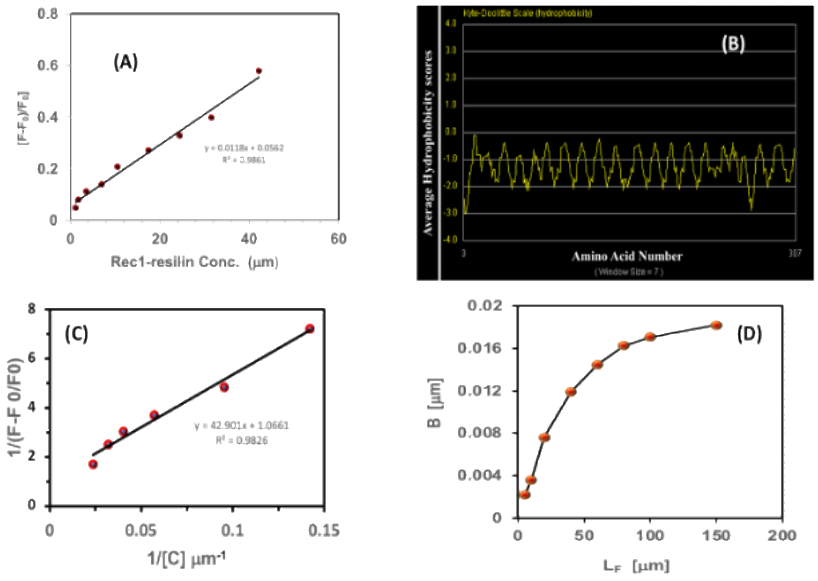

Figure S11: **Surface hydrophobicity of Rec1-resilin and binding interaction .of ANS to Rec1-resilin.** (A) The surface hydrophobicity (SH) plot of Rec1-resilin. Since fluorescence intensity is

an arbitrary unit, the quantity "relative fluorescence" (F_R) defined as $F_R = (F - F_0)/F_0$ is used. The slope of the curve determined using least-squares linear regression is considered as an index of SH and appears to be very low. (B) Kyte-Doolittle (K-D) hydrophobicity plot of Rec1-resilin using amino acid sequence (Figure S2) with window size 7. A score of 4.6 is the most hydrophobic and a score of - 4.6 is the most hydrophilic hydrophobicity score according to the K-D plot. All the regions of Rec1-resilin exhibit values below zero reflecting the high hydrophilicity of the protein surface and experimentally supports Kyte-Doolittle (K-D) hydrophobicity plot (A). (C) A double-reciprocal plot of $1/(\lambda_{max})$ vs 1/[C]. The increase in the fluorescence intensity, λ_{max} (ΔF^*) per mM-ANS bound was calculated using this plot. Using the calibration factor deduced from the curve, the detected increase in fluorescence intensity (ΔF) was converted into mM of bound ANS. (D) Plot of bound ligand (B) vs. total free ligand (L_F). The curve obtained is smooth and has no inflection points, maxima, or minima and reflects the quality of the data.

S12: Fluorescence titration of various Rec1-resilin by ANS both in the presence and in the absence of different types and levels of crowders

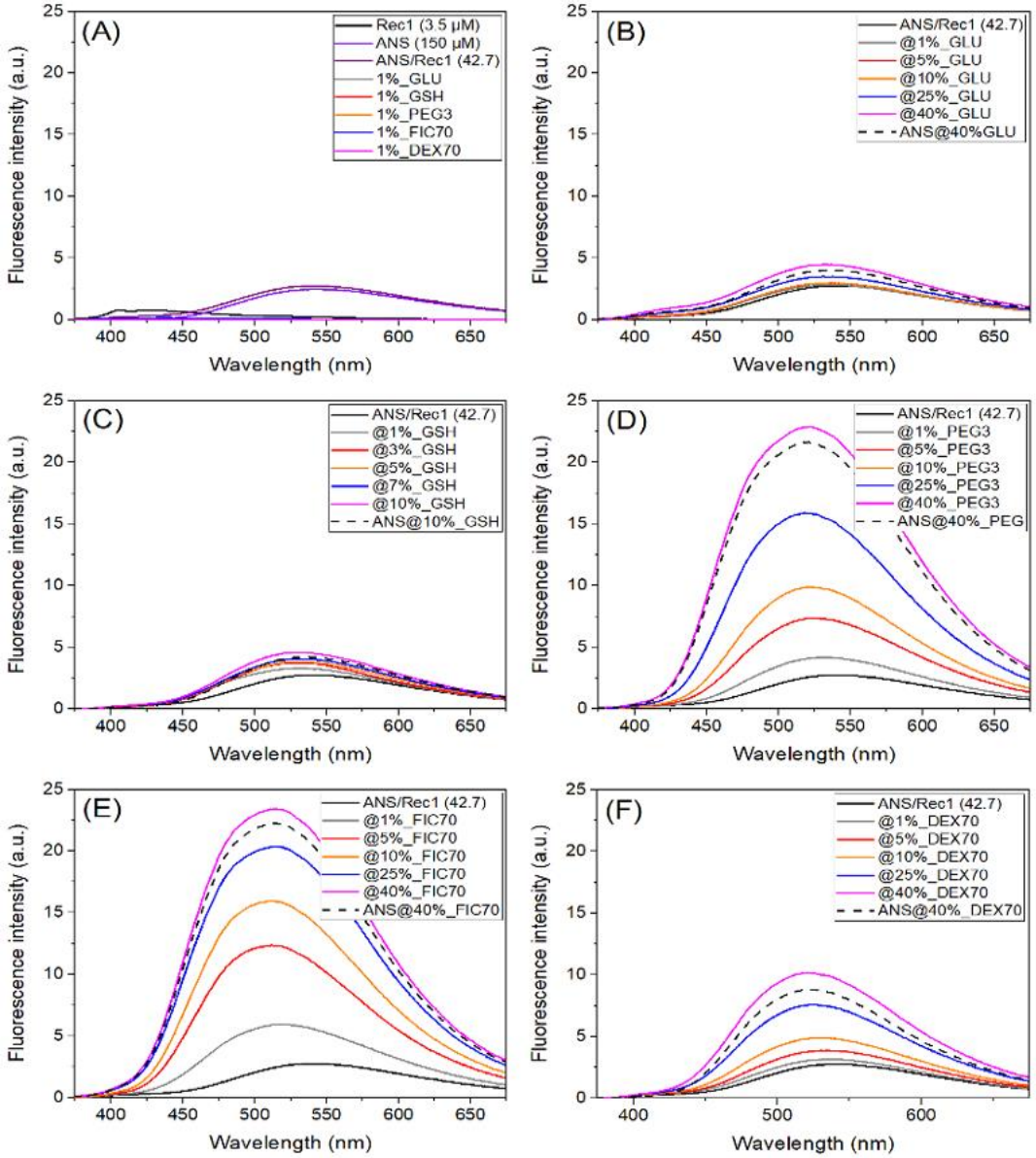

Figure S12: **Fluorescence titration of various Rec1-resilin by ANS both in the presence and the absence of different types and levels of crowders.** Fluorescence spectra of (A) pure Rec1-resilin, ANS, (at optimal molar ratio), and crowding agents. Free ANS in aqueous solution displays a negligible fluorescence intensity with λ_{max} ~543. (B-D) Fluorescence emission spectra of ANS/Rec1-resilin (at fixed molar ratio) as a function of different crowding agent at different concentration: (B) glucose (GLU), (C) glutathione (GSH), (D) polyethylene glycol (PEG3), (E) Ficoll (FIC70), and (F) dextran (DEX70). Both restricted mobility and hydrophobicity of the nearest environment of ANS contribute significantly to the increased fluorescence intensity.

S13: Assessment of the conformational change using Tyr amino acid residue as the intrinsic fluorescence probe

Rec1-resilin lacks the tryptophan (Trp) amino acid residue, and the fluorescence emission in Rec1-resilin is entirely due to Tyr. In *rec1-resilin*, the natural fluorophore *Tyr* is present in two major distinctly different tripeptide environments, which are respectively ***Ser-Tyr-Gly*** (*Ser21-Tyr22-Gly23, Ser37-Tyr38-Gly39, Ser52-Tyr53-Gly54, Ser76-Tyr77-Gly78, Ser93-Tyr94-Gly95, Ser141-Tyr142-Gly143, Ser160-Tyr161-Gly162, Ser206-Tyr207-Gly208, Ser240-Tyr241-Gly242, Ser258-Tyr259-Gly260, Ser271-Tyr272-Gly273, Ser288-Tyr289-Gly290, Ser303-Tyr304-Gly305*= **total 13**) and ***Thr-Tyr-Gly*** (*Thr108-Tyr109-Gly110,Thr123-Tyr124-Gly125,Thr175-Tyr176-Gly177,Thr190-Tyr191-Gly192, Thr221-Tyr222-Gly223*= **total 5**); with one each of *Ser14-Tyr15-Leu16*, and *Gly68-Tyr69-Ala70*. In the case of Rec1-resilin the observation of a single absorption band with peak at 275 nm confirms the presence of *Tyr* in the neutral form.

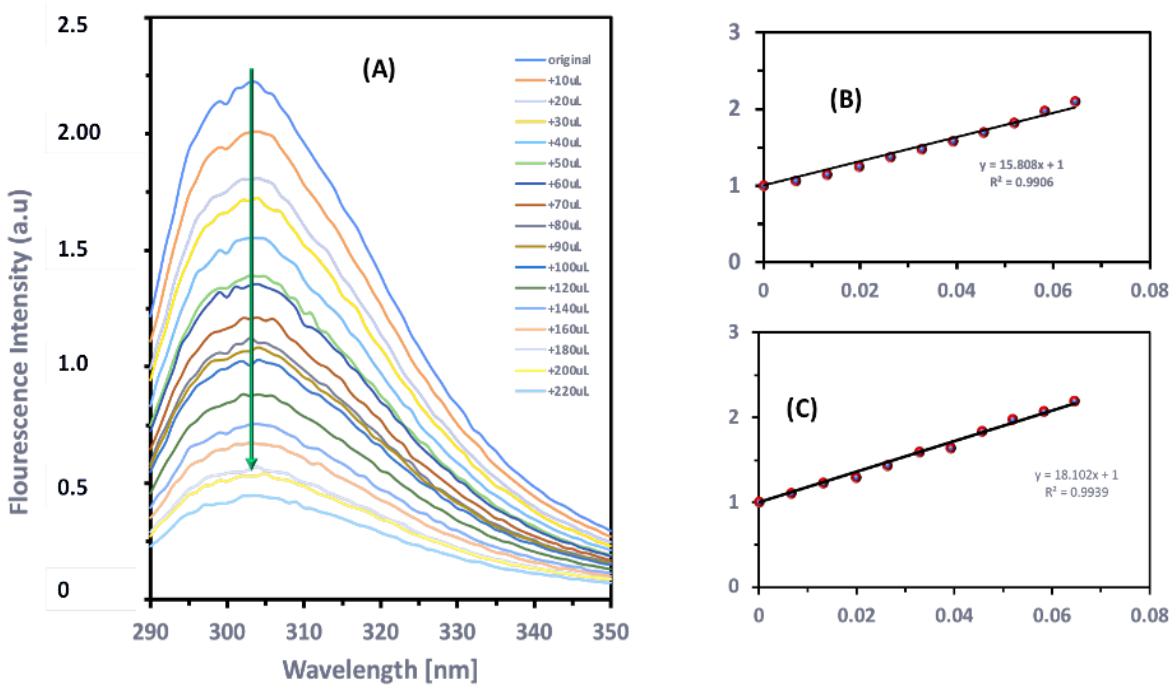

Figure S13: **Assessment of the conformational change using tyrosine amino acid residue (Tyr) as the intrinsic fluorescence probe**. (A) Typical fluorescence quenching experiments of Rec1-resilin using Ficoll (25mg/ml) as crowder and adding acrylamide as an external fluorescence quencher. The data were analyzed according to the modified Stern-Volmer relation :

$$\frac{F_0}{F} = 1 + KSV\,[Q] \quad (S3)$$

where F_0 and F are the fluorescence intensities in the absence and presence of quencher, [Q] is the concentration of quencher, and K_{SV} is the Stern-Volmer constant. (B) Stern-Volmer plots of the acrylamide quenching of Tyr in pure Rec1-resilin in absence of crowder and in (C) presence of a crowder (25mg/ml Ficoll). The resulting Stern-Volmer plots were linear in all cases and Stern Volmer quenching constants (K_{SV}) were calculated from the linear-fits of the data.

S14: Quantitative estimation of the secondary structure(s) from the CD spectra

Table S1. CD spectrum deconvolution fit parameters. The analysis was performed using DichroWeb with CONTIN algorithm and reference set 7 (containing some unordered model proteins).

Sample*	Helix	Strand	Turns	Unordered
Rec1	0.064	0.162	0.136	0.638
Rec1@1%GLU	0.048	0.170	0.113	0.668
Rec1@2.5%GLU	0.097	0.110	0.160	0.633
Rec1@0.01%GSH	0.056	0.155	0.119	0.670
Rec1@0.05%GSH	0.049	0.339	0.186	0.427
Rec1@1%PEG3	0.041	0.215	0.119	0.625
Rec1@2.5%PEG3	0.054	0.181	0.125	0.639
Rec1@1%FIC70	0.057	0.199	0.137	0.607
Rec1@2.5%FIC70	0.061	0.196	0.147	0.596
Rec1@1%DEX70	0.069	0.172	0.147	0.612
Rec1@2.5%DEX70	0.074	0.200	0.162	0.564

*The analysis could not be performed for samples with high crowder concentration (10% GSH and 40% for other crowders) as the lowest wavelength datapoint required to perform the analysis was 190 nm.

S15*:* Amino acid composition of Rec1-resilin

Table S2. Amino acid composition of Rec1-resilin.

Amino acids		Symbol	No. of units	Mol%
Non-polar side chain	Glycine	Gly/G	104	33.5
	Alanine	Ala/A	19	6.1
	Valine	Val/V	1	0.3
	Leucine	Leu/L	2	0.6
	Isoleucine	Ile/I	-	-
	Methionine	Met/M	-	-
	Proline	Pro/P	42	13.5
	Phenylalanine	Phe/F	1	0.3
	Tryptophan	Try/W	-	-
	Subtotal		**169**	**54.5**
Uncharged polar side chain	Serine	Ser/S	44	14.2
	Threonine	Thr/T	6	1.9
	Asparagine	Asn/N	20	6.4
	Glutamine	Gln/Q	13	4.2
	Tyrosine	Tyr/Y	21	6.8
	Cysteine	Cys/C	-	-
	Subtotal		**104**	**33.5**
Charged polar side chain	Lysine	Lys/K	2	0.6
	Arginine	Arg/R	16	5.2
	Histidine	His/H	6	1.9
	Aspartic acid	Asp/D	12	3.9
	Glutamic acid	Glu/E	1	0.3
	Subtotal		**37**	**11.9**
Total			**310**	**100**

S16: Density values of aqueous crowding agent solutions as a function of solute concentration used to calculate volume fraction

Table S3. Density values of aqueous crowding agent solutions as a function of solute concentration used to calculate volume fraction (ϕ) using the relationship ϕ = (wt%)/(100*density).

Molecule	Concentration (wt%)	Density (g/cc)
GLU[76]	5	1.017
	10	1.038
	25	1.108
	40	1.177
GSH	1	1.004
	5	1.019
	7.5	1.028
	10	1.038
PEG3[77]	5	1.003
	10	1.012
	25	1.038
	40	1.067
FIC70[78]	5	1.018
	10	1.032
	18	1.060
	25	1.078
	40	1.135
DEX70[78]	5	1.020
	10	1.035
	25	1.088
	40	1.150

S17: Size values of D-Rec1 and crowder molecules in 10 mM PBS

Table S4. Size values of D-Rec1 and crowder molecules in 10 mM PBS. The hydrodynamic diameter (D_h) of all samples (0.5 wt%) were measured using DLS. The radius of gyration (R_g) of D-Rec1 (3 wt%) was measured using SANS, and crowder molecules (0.5 wt%) using SAXS.

Molecule	D_h **(nm)**	R_g **(nm) obtained from**		
		Model function fits	**Guinier approximation**	**P(r) function fits**
D-Rec1	10.8 ± 0.2	6.2 ± 0.1	6.5 ± 0.3	7.4
GLU	1.1 ± 0.1	0.43*	0.43*	0.43*
GSH	4.3 ± 0.1	1.1 ± 0.1	1.1 ± 0.1	1.1**
PEG3	5.8 ± 0.1	2.2 ± 0.2	1.7 ± 0.1	1.8
FIC70	9.8 ± 0.2	4.4 ± 0.2	4.1 ± 0.1	4.3
DEX70	13.4 ± 0.4	6.5 ± 0.2	6.3 ± 0.2	6.3

*value taken from half the kinetic diameter[42] **value from model function fits

S18: Model parameters fitted to the experimental data.

Table S5. Model parameters fitted to the experimental data.

Parameter	**DEX 70**	**FIC70**	**PEG3**	**GSH**	**GLU**	**D-Rec1**
a - Crowder Size (nm)	6.30	4.30	1.80	1.10	0.43	7.40
η - Density of Crowder Surface Atoms (#/A^2)	0.60	0.95	1.30	0.75	0.05	0.35
k1 - Rate of dielectric constant with Crowder (-)	19.00	0.95	0.95	2.00	0.50	0.10
φ1 - Multiplier of dielectric constant with Crowder (-)	2.50	2.20	1.54	2.00	1.50	1.00
k2 - Rate of Crowder-Resilin Interactions (-)	0.20	0.15	0.15	0.40	0.20	0.20
φ2 - Multiplier of Crowder-Resilin Interactions (-)	100.0	7.3	7.3	7.0	10.0	5.0
k3 - Rate of Entropy Loss with Crowder (-)	0.005	0.008	0.010	0.015	0.004	0.100
φ3 - Multiplier of Entropy Loss with Crowder (-)	3000	100	130	100	60	28
b - Average distance between nodes in Resilin (A)	7.64	7.64	7.64	7.64	7.64	7.64
N_{nodes} - Number of nodes in Resilin (#)	11.2	11.2	11.2	11.2	11.2	11.2
ϵ - Dielectric constant	100	100	100	100	100	100
R^2 - Goodness of Fit	0.988	0.946	0.547	0.795	0.512	0.960
RMSE - Root Mean Squared Error	0.453	0.651	1.935	0.597	0.552	0.257

S19: ESI electrospray ionization time-of-flight mass spectrometry

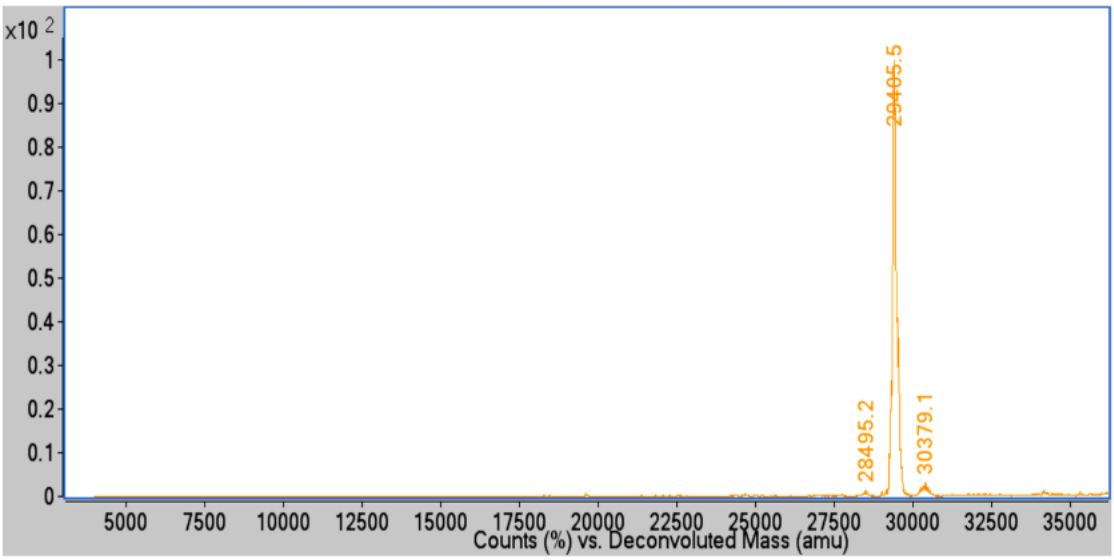

Figure S14. ESI-ToF mass spectra of bio-synthesized D-Rec1. Molecular weight of D-Rec1 (29.5 kDa) is larger than protonated Rec1-resilin (28.5 kDa) and indicates deuteration on non-exchangeable hydrogen positions in the protein.

REFERENCES AND NOTES

1. K. A. Sharp, Unpacking the origins of in-cell crowding. *Proc. Natl. Acad. Sci. U.S.A.* **113**, 1684–1685 (2016).

2. I. M. Kuznetsova, K. K. Turoverov, V. N. Uversky, What macromolecular crowding can do to a protein. *Int. J. Mol. Sci.* **15**, 23090–23140 (2014).

3. Y. Wang, M. Sarkar, A. E. Smith, A. S. Krois, G. J. Pielak, Macromolecular crowding and protein stability. *J. Am. Chem. Soc.* **134**, 16614–16618 (2012).

4. Y. Phillip, G. Schreiber, Formation of protein complexes in crowded environments—From in vitro to in vivo. *FEBS Lett.* **587**, 1046–1052 (2013).

5. H.-X. Zhou, S. Qin, Simulation and modeling of crowding effects on the thermodynamic and kinetic properties of proteins with atomic details. *Biophys. Rev.* **5**, 207–215 (2013).

6. S. Shahid, M. I. Hassan, A. Islam, F. Ahmad, Size-dependent studies of macromolecular crowding on the thermodynamic stability, structure and functional activity of proteins: In vitro and in silico approaches. *Biochim. Biophys. Acta Gen. Subj.* **1861**, 178–197 (2017).

7. P. E. Wright, H. J. Dyson, Intrinsically disordered proteins in cellular signalling and regulation. *Nat. Rev. Mol. Cell Biol.* **16**, 18–29 (2015).

8. J. Liu, N. B. Perumal, C. J. Oldfield, E. W. Su, V. N. Uversky, A. K. Dunker, Intrinsic disorder in transcription factors. *Biochemistry* **45**, 6873–6888 (2006).

9. A. L. Darling, Y. Liu, C. J. Oldfield, V. N. Uversky, Intrinsically disordered proteome of human membrane-less organelles. *Proteomics* **18**, 1700193 (2018).

10. H. Popelka, Dancing while self-eating: Protein intrinsic disorder in autophagy. *Prog. Mol. Biol. Transl. Sci.* **174**, 263–305 (2020).

11. V. N. Uversky, C. J. Oldfield, A. K. Dunker, Intrinsically disordered proteins in human diseases: Introducing the D^2 concept. *Annu. Rev. Biophys.* **37,** 215–246 (2008).

12. R. Tenchov, Q. A. Zhou, Intrinsically disordered proteins: Perspective on COVID-19 infection and drug discovery. *ACS Infect. Dis.* **8**, 422–432 (2022).

13. A. V. Fonin, A. L. Darling, I. M. Kuznetsova, K. K. Turoverov, V. N. Uversky, Intrinsically disordered proteins in crowded milieu: When chaos prevails within the cellular gumbo. *Cell. Mol. Life Sci.* **75**, 3907–3929 (2018).

14. S. Qin, H.-X. Zhou, Effects of macromolecular crowding on the conformational ensembles of disordered proteins. *J. Phys. Chem. Lett.* **4**, 3429–3434 (2013).

15. E. A. Cino, M. Karttunen, W.-Y. Choy, Effects of molecular crowding on the dynamics of intrinsically disordered proteins. *PLOS ONE* **7**, e49876 (2012).

16. A. Soranno, I. Koenig, M. B. Borgia, H. Hofmann, F. Zosel, D. Nettels, B. Schuler, Single-molecule spectroscopy reveals polymer effects of disordered proteins in crowded environments. *Proc. Natl. Acad. Sci. U.S.A.* **111**, 4874–4879 (2014).

17. A. Banks, S. Qin, K. L. Weiss, C. B. Stanley, H.-X. Zhou, Intrinsically disordered protein exhibits both compaction and expansion under macromolecular crowding. *Biophys. J.* **114**, 1067–1079 (2018).

18. K. Lindorff-Larsen, N. Trbovic, P. Maragakis, S. Piana, D. E. Shaw, Structure and dynamics of an unfolded protein examined by molecular dynamics simulation. *J. Am. Chem. Soc.* **134**, 3787–3791 (2012).

19. R. E. Ithuralde, A. E. Roitberg, A. G. Turjanski, Structured and unstructured binding of an intrinsically disordered protein as revealed by atomistic simulations. *J. Am. Chem. Soc.* **138**, 8742–8751 (2016).

20. W. Adamski, N. Salvi, D. Maurin, J. Magnat, S. Milles, M. R. Jensen, A. Abyzov, C. J. Moreau, M. A. Blackledge, A unified description of intrinsically disordered protein dynamics under physiological conditions using NMR spectroscopy. *J. Am. Chem. Soc.* **141**, 17817–17829 (2019).

21. E. Delaforge, J. Kragelj, L. Tengo, A. Palencia, S. Milles, G. Bouvignies, N. Salvi, M. Blackledge, M. R. Jensen, Deciphering the dynamic interaction profile of an intrinsically disordered protein by NMR exchange spectroscopy. *J. Am. Chem. Soc.* **140**, 1148–1158 (2018).

22. J.-B. Guilbaud, A. Saiani, Using small angle scattering (SAS) to structurally characterise peptide and protein self-assembled materials. *Chem. Soc. Rev.* **40,** 1200–1210 (2011).

23. R. Balu, J. P. Mata, R. Knott, C. M. Elvin, A. J. Hill, N. R. Choudhury, N. K. Dutta, Effects of crowding and environment on the evolution of conformational ensembles of the multi-stimuli-responsive intrinsically disordered protein, Rec1-resilin: A small-angle scattering investigation. *J. Phys. Chem. B,* **120**, 6490–6503 (2016).

24. J. L. Whittaker, R. Balu, R. Knott, L. de Campo, J. P. Mata, C. Rehm, A. J. Hill, N. K. Dutta, N. Roy Choudhury, Structural evolution of photocrosslinked silk fibroin and silk fibroin-based hybrid hydrogels: A small angle and ultra-small angle scattering investigation. *Int. J. Biol. Macromol.* **114**, 998–1007 (2018).

25. W. T. Heller, Small-angle neutron scattering and contrast variation: A powerful combination for studying biological structures. *Acta Crystallogr. D Struct. Biol. Crystallogr.* **66**, 1213–1217 (2010).

26. D. W. Schaefer, M. M. Agamalian, Ultra-small-angle neutron scattering: A new tool for materials research. *Curr. Opin. Solid State Mater. Sci.* **8**, 39–47 (2004).

27. E. Appel, J. Michels, S. N. Gorb, Native resilin: Properties, occurrence and biological functions of a remarkable bio-elastomer, in *Biomimetic Protein Based Elastomers: Emerging Materials for the Future*, N. Roy Choudhury, J. C. Liu, N. K. Dutta, Eds. (RSC, 2022), pp. 8–44.

28. R. Balu, N. K. Dutta, A. K. Dutta, N. R. Choudhury, Resilin-mimetics as a smart biomaterial platform for biomedical applications. *Nat. Commun.* **12**, 149 (2021).

29. R. Balu, R. Knott, N. P. Cowieson, C. M. Elvin, A. J. Hill, N. R. Choudhury, N. K. Dutta, Structural ensembles reveal intrinsic disorder for the multi-stimuli responsive bio-mimetic protein Rec1-resilin. *Sci. Rep.* **5**, 10896 (2015).

30. N. K. Dutta, M. Y. Truong, S. Mayavan, N. Roy Choudhury, C. M. Elvin, M. Kim, R. Knott, K. M. Nairn, A. J. Hill, A genetically engineered protein responsive to multiple stimuli. *Angew. Chem. Int. Ed.* **50**, 4428–4431 (2011).

31. N. K. Dutta, N. R. Choudhury, M. Y. Truong, M. Kim, C. M. Elvin, A. J. Hill, Physical approaches for fabrication of organized nanostructure of resilin-mimetic elastic protein rec1-resilin. *Biomaterials* **30**, 4868–4876 (2009).

32. M. Y. Truong, N. K. Dutta, N. R. Choudhury, M. Kim, C. M. Elvin, A. J. Hill, B. Thierry, K. A. Vasilev, A pH-responsive interface derived from resilin-mimetic protein *Rec1-resilin*. *Biomaterials* **31**, 4434–4446 (2010).

33. M. Y. Truong, N. K. Dutta, N. R. Choudhury, M. Kim, C. M. Elvin, K. M. Nairn, A. J. Hill, The effect of hydration on molecular chain mobility and the viscoelastic behavior of resilin-mimetic protein-based hydrogels. *Biomaterials* **32**, 8462–8473 (2011).

34. R. Balu, P. Dorishetty, J. P. Mata, A. J. Hill, N. K. Dutta, N. R. Choudhury, Tuning the hierarchical structure and resilience of resilin-like polypeptide hydrogels using graphene oxide. *ACS Appl. Bio Mater.* **3**, 8688–8697 (2020).

35. S. Mayavan, N. K. Dutta, N. R. Choudhury, M. Kim, C. M. Elvin, A. J. Hill, Self-organization, interfacial interaction and photophysical properties of gold nanoparticle complexes derived from resilin-mimetic fluorescent protein *rec1-resilin*. *Biomaterials* **32**, 2786–2796 (2011).

36. N. K. Dutta, N. Roy Choudhury, S. Mayavan, R. Balu, J. Whittaker, C. Elvin, A. J. Hill, Template directed formation of metal nanoparticles and uses thereof, WO Patent 2014071463A1 (2014).

37. R. Balu, L. Bourgeois, C. M. Elvin, A. J. Hill, N. R. Choudhury, N. K. Dutta, A multi-responsive intrinsically disordered protein (IDP)-directed green synthesis of fluorescent gold nanoclusters. *J. Mater. Chem. B* **3**, 6580–6586 (2015).

38. N. K. Dutta, N. Roy Choudhury, R. Balu, C. Elvin, A. J. Hill, Formation of sub-nano metal particles, WO Patent 20150240631A1 (2015).

39. R. Balu, R. Knott, C. M. Elvin, A. J. Hill, N. Roy Choudhury, N. K. Dutta, A sustainable biomineralization approach for the synthesis of highly fluorescent ultra-small Pt nanoclusters. *Biosensors* **9,** 128 (2019).

40. D. I. Svergun, M. H. J. Koch, P. A. Timmins, R. P. May, *Small Angle X-Ray and Neutron Scattering from Solutions of Biological Macromolecules* (Oxford Univ. Press, 2013).

41. M. E. Oates, P. Romero, T. Ishida, M. Ghalwash, M. J. Mizianty, B. Xue, Z. Dosztányi, V. N. Uversky, Z. Obradovic, L. Kurgan, A. K. Dunker, J. Gough, D^2P^2: Database of disordered protein predictions. *Nucleic Acids Res.* **41**, D508–D516 (2013).

42. S. Li, V. A. Tuan, J. L. Falconer, R. D. Noble, Separation of 1,3-propanediol from glycerol and glucose using a ZSM-5 zeolite membrane. *J. Membr. Sci.* **191**, 53–59 (2001).

43. C. D. Putnam, M. Hammel, G. L. Hura, J. A. Tainer, X-ray solution scattering (SAXS) combined with crystallography and computation: Defining accurate macromolecular structures, conformations and assemblies in solution. *Q. Rev. Biophys.* **40**, 191–285 (2007).

44. B. Hammouda, SANS from homogeneous polymer mixtures: A unified overview, in *Polymer Characteristics* (Springer, 1993), pp. 87–133.

45. V. Petrenko, L. Bulavin, M. Avdeev, V. Garamus, M. Koneracka, P. Kopcansky, Structure and interaction of poly(ethylene glycol) in aqueous solutions. Small-angle neutron scattering data. *Macromol. Symp.* **335**, 20–23 (2014).

46. P. Bernadó, Effect of interdomain dynamics on the structure determination of modular proteins by small-angle scattering. *Eur. Biophys. J.* **39**, 769–780 (2010).

47. D. I. Svergun, M. V. Petoukhov, M. H. J. Koch, Determination of domain structure of proteins from X-ray solution scattering. *Biophys. J.* **80**, 2946–2953 (2001).

48. E. F. Pettersen, T. D. Goddard, C. C. Huang, G. S. Couch, D. M. Greenblatt, E. C. Meng, T. E. Ferrin, UCSF Chimera—A visualization system for exploratory research and analysis. *J. Comput. Chem.* **25**, 1605–1612 (2004).

49. M. Cardamone, N. K. Puri, Spectrofluorimetric assessment of the surface hydrophobicity of proteins. *Biochem. J.* **282**, 589–593 (1992).

50. A. Biswas, K. P. Das, Zn^{2+} enhances the molecular chaperone function and stability of α-crystallin. *Biochemistry* **47**, 804–816 (2008).

51. M. R. Eftink, C. A. Ghiron, Fluorescence quenching studies with proteins. *Anal. Biochem.* **114**, 199–227 (1981).

52. N. J. Greenfield, Using circular dichroism spectra to estimate protein secondary structure. *Nat. Protoc.* **1**, 2876–2890 (2006).

53. A. J. Miles, S. G. Ramalli, B. A. Wallace, DichroWeb, a website for calculating protein secondary structure from circular dichroism spectroscopic data. *Protein Sci.* **31**, 37–46 (2021).

54. Y. C. Kim, J. Mittal, Crowding induced entropy-enthalpy compensation in protein association equilibria. *Phys. Rev. Lett.* **110**, 208102 (2013).

55. I. M. Kuznetsova, B. Y. Zaslavsky, L. Breydo, K. K. Turoverov, V. N. Uversky, Beyond the excluded volume effects: Mechanistic complexity of the crowded milieu. *Molecules* **20**, 1377–1409 (2015).

56. M. Sarkar, C. Li, G. J. Pielak, Soft interactions and crowding. *Biophys. Rev.* **5**, 187–194 (2013).

57. G. Rivas, A. P. Minton, Macromolecular crowding in vitro, in vivo, and in between. *Trends Biochem. Sci.* **41**, 970–981(2016).

58. A. Christiansen, P. Wittung-Stafshede, Synthetic crowding agent dextran causes excluded volume interactions exclusively to tracer protein apoazurin. *FEBS Lett.* **588**, 811–814 (2014).

59. J. Rosen, Y. C. Kim, J. Mittal, Modest protein−crowder attractive interactions can counteract enhancement of protein association by intermolecular excluded volume interactions. *J. Phys. Chem. B* **115**, 2683–2689 (2011).

60. N. Kozer, Y. Y. Kuttner, G. Haran, G. Schreiber, Protein-protein association in polymer solutions: From dilute to semidilute to concentrated. *Biophys. J.* **92**, 2139–2149 (2007).

61. C. M. Miller, Y. C. Kim, J. Mittal, Protein composition determines the effect of crowding on the properties of disordered proteins. *Biophys. J.* **111**, 28–37 (2016).

62. H. Kang, P. A. Pincus, C. Hyeon, D. Thirumalai, Effects of macromolecular crowding on the collapse of biopolymers. *Phys. Rev. Lett.* **114**, 068303 (2015).

63. P. P. Bansal, A. J. Ardell, Average nearest-neighbor distances between uniformly distributed finite particles. *Metallography* **5**, 97–111(1972).

64. L. Sapir, D. Harries, Is the depletion force entropic? Molecular crowding beyond steric interactions. *Curr. Opin. Colloid Interface Sci.* **20**, 3–10 (2015).

65. H. Kobayashi, R. G. Winkler, Universal conformational properties of polymers in ionic nanogels. *Sci. Rep.* **6**, 19836 (2016).

66. H.-X. Zhou, G. Rivas, A. P. Minton, Macromolecular crowding and confinement: Biochemical, biophysical, and potential physiological consequences. *Annu. Rev. Biophys.* **37**, 375–397 (2008).

67. D. Baowan, J. M. Hill, Mathematical modeling of interaction energies between nanoscale objects: A review of nanotechnology applications. *Adv. Mech. Eng.* **8**, 1–16 (2016).

68. X. Wang, S. Ramírez-Hinestrosa, J. Dobnikar, D. Frenkel, The Lennard-Jones potential: When (not) to use it. *Phys. Chem. Chem. Phys.* **22**, 10624–10633 (2020).

69. A. P. Duff, K. L. Wilde, A. Rekas, V. Lake, P. J. Holden, Robust high-yield methodologies for ^{2}H and $^{2}H/^{15}N/^{13}C$ labeling of proteins for structural investigations using neutron scattering and NMR. *Methods Enzymol.* **563**, 3–25 (2015).

70. M. Kim, C. Elvin, A. Brownlee, R. Lyons, High yield expression of recombinant pro-resilin: Lactose-induced fermentation in *E. coli* and facile purification. *Protein Expr. Purif.* **52**, 230–236 (2007).

71. K. Wood, J. P. Mata, C. J. Garvey, C.-M. Wu, W. A. Hamilton, P. Abbeywick, D. Bartlett, F. Bartsch, P. Baxter, N. Booth, W. Brown, J. Christoforidis, D. Clowes, T. d'Adam, F. Darmann, M. Deura, S. Harrison, N. Hauser, G. Horton, D. Federici, F. Franceschini, P. Hanson, E. Imamovic, P. Imperia, M. Jones, S. Kennedy, S. Kim, T. Lam, W. T. Lee, M. Lesha, D. Mannicke, T. Noakes, S. R. Olsen, J. C. Osborn, D. Penny, M. Perry, S. A. Pullen, R. A. Robinson, J. C. Schulz, N. Xiong, E. P. Gilbert, QUOKKA, the pinhole small-angle neutron scattering instrument at the OPAL Research Reactor, Australia: Design, performance, operation and scientific highlights. *J. Appl. Cryst.* **51**, 294–314 (2018).

72. S. R. Kline, Reduction and analysis of SANS and USANS data using IGOR Pro. *J. Appl. Cryst.* **39**, 895–900 (2006).

73. P. V. Konarev, V. V. Volkov, A. V. Sokolova, M. H. J. Koch, D. I. Svergun, PRIMUS: A Windows PC-based system for small-angle scattering data analysis. *J. Appl. Cryst.* **36**, 1277–1282 (2003).

74. R. Balu, N. Roy Choudhury, J. P. Mata, L. de Campo, C. Rehm, A. J. Hill, N. K. Dutta, Evolution of the interfacial structure of a catalyst Ink with the quality of the dispersing solvent: A contrast variation small-angle and ultrasmall-angle neutron scattering investigation. *ACS Appl. Mater. Interfaces* **11**, 9934–9946 (2019).

75. A. Brûlé, F. Darmann, F. Bartsch, A. Berry, Design and performance of the variable-wavelength Bonse–Hart ultra-small-angle neutron scattering diffractometer KOOKABURRA at ANSTO. *J. Appl. Cryst.* **51**, 1–8 (2018).

76. J. F. Comesaña, J. J. Otero, E. García, A. Correa, Densities and viscosities of ternary systems of water + glucose + sodium chloride at several temperatures. *J. Chem. Eng. Data* **48**, 362–366 (2003).

77. A. Eliassi, H. Modarress, G. A. Mansoori, Densities of poly(ethylene glycol) + water mixtures in the 298.15−328.15 K temperature range. *J. Chem. Eng. Data* **43**, 719–721 (1998).

78. O. Mach, L. Lacko, Density gradient in a dextran medium. *Anal. Biochem.* **22**, 393–397 (1968).